Identification of the Structure of the Bi Promoted Pt Non-oxidative Coupling of Methane Catalyst: A Nanoscale Pt3Bi Intermetallic Alloy

Journal:	*Catalysis Science & Technology*
Manuscript ID	CY-COM-10-2018-002171.R1
Article Type:	Paper
Date Submitted by the Author:	18-Dec-2018
Complete List of Authors:	ZhuChen, Johnny; Purdue University, Davidon School of Chemical Engineering Wu, Zhenwei; Purdue University, Davidson School of Chemical Engineering; Stanford University, School of Chemical Engineering Zhang, Xiaoben; Dalian Institute of Chemical Physics, Microscopy Research Lab Choi, Slgi; Purdue University, Davidson School of Chemical Engineering Xiao, Yang; Purdue University, Davidson School of Chemical Engineering Varma, Arvind; Purdue University, Davidson School of Chemical Engineering Liu, Wei; Dalian Institute of Chemical Physics, Microscopy Research Lab Zhang, Guanghui; Dalian University of Technology; Purdue University, Davidson School of Chemical Engineering Miller, Jeffrey T.; Purdue University, Davidson School of Chemical Engineering

SCHOLARONE™
Manuscripts

ARTICLE

Identification of the Structure of the Bi Promoted Pt Non-oxidative Coupling of Methane Catalyst: A Nanoscale Pt₃Bi Intermetallic Alloy

Johnny Zhu Chen,[a] Zhenwei Wu,[a,b] Xiaoben Zhang,[c] Slgi Choi,[a] Yang Xiao,[a] Arvind Varma,[a] Wei Liu,[c] Guanghui Zhang,*[a,d] and Jeffrey T. Miller*[a]

Recently, stable non-oxidative conversion of methane (NOCM) for up to 8 h with a C_2 selectivity greater than 90% has been reported over Pt-Bi/ZSM-5 at moderate temperatures (600-700°C). In this study, we show that the structure of the bimetallic nanoparticles on Pt-Bi/ZSM-5 catalyst is similar to Pt-Bi/SiO$_2$. EXAFS indicates the formation of Pt-rich bimetallic Pt-Bi nanoparticles with Pt-Bi bond distance of 2.80 Å. The XRD spectra (on SiO$_2$) are consistent with cubic, intermetallic surface Pt$_3$Bi phase on a Pt core. The Pt$_3$Bi structure is not known in the thermodynamic phase diagram. In all catalysts, only a small fraction of Bi alloys with Pt. At high Bi loadings, excess Bi reduces at high temperature, covering the catalytic surface leading to a loss in activity. At lower Bi loadings with little excess Bi, the Pt$_3$Bi surface is effective for non-oxidative coupling of CH_4 (on ZSM-5) and propane dehydrogenation (on SiO$_2$).

Introduction

Shale gas has been widely exploited in the United States, and catalytic conversion of shale gas has received increasing attention in the past decade.[1, 2] Methane is the major component of shale gas (>70%) and natural gas (~95%),[3] which is mainly used for electricity and power generation. Chemical utilization of methane is primarily for production of hydrogen and syngas (CO+H$_2$), which may be further converted to methanol, ammonia, etc. Direct conversion of methane to fuels and value-added chemicals holds promising potential as an alternative to production of these from petroleum.[4]

One option, which has been widely studied, is the oxidative coupling of methane (OCM) to ethane and ethylene that are important industrial intermediates for production of fuels and chemicals.[5-7] The OCM reaction, however, often leads to over-oxidation to CO and CO$_2$, giving low selectivity toward hydrocarbon products.[8] To avoid over-oxidation, non-oxidative conversion of methane (NOCM) has also been studied since Wang et al. reported 7.2% conversion of methane over Mo/ZSM-5 to benzene and other aromatics. [9-13]

The reaction, however, has a high coke selectivity (~50%), which blocks the zeolite pores and MoC$_x$ surface, leading to deactivation of the catalyst within a few hours.[14] Although Mo/ZSM-5 has been extensively studied, few other catalysts are known to catalyze NOCM. Guo et al. showed that Fe embedded in silica matrix converts methane to ethylene and aromatics at 1363 K with sustained conversion as high as 50%.[15] Pt catalysts have also been reported, but with limited success. Belgued et al. reported that Pt/SiO$_2$ could convert methane to ethane.[16] The lifetime, however, was approximately 10 minutes due to the rapid formation of coke. The selectivity to C$_2$ was also poor at about 20%. The catalyst lifetime was significantly improved to over 10 h with over 85% C$_2$ selectivity using a Pt-Sn catalyst.[17] The conversion, however, was lower than 0.3% with this catalyst. More recently Xiao and Varma reported stable methane conversion at 2% with C$_2$ selectivity greater than 90% for up to 8 h over Pt-Bi/ZSM-5 at moderate temperatures (600-700°C).[18] The optimum conversion was obtained with 0.8Bi-1Pt/ZSM-5; while with higher Bi loadings, there was little activity. Higher reaction temperatures also gave lower activity. The detailed structure of this catalyst, however, was not investigated. Determination of the catalyst structure and the role of Bi in promoting Pt are essential for understanding the structure-activity relationship and will provide useful guidance for rational design of improved NOCM catalysts.

Herein we report the characterization of the bimetallic Pt-Bi/ZSM-5 NOCM catalysts and similar Pt-Bi/SiO$_2$. The latter is also selective for propane dehydrogenation. *In situ* X-ray absorption spectroscopy (XAS), *In situ* Fourier transform infrared (FTIR), high-angle annular dark field scanning

[a] Davidson School of Chemical Engineering, Purdue University, 480 Stadium Mall Drive, IN 47906, United States.
[b] School of Chemical Engineering, Stanford University, 381 North-South Mall, Stanford, CA 94305, United States.
[c] Dalian Institute of Chemical Physics, Chinese Academy of Sciences, Dalian, Liaoning 116023, China
[d] State Key Laboratory of Fine Chemicals, PSU-DUT Joint Center for Energy Research, School of Chemical Engineering, Dalian University of Technology, Dalian, Liaoning 116024, China
gzhang@dlut.edu.cn (G. Zhang); mill1194@purdue.edu (J.T. Miller)
Electronic Supplementary Information (ESI) available: [EXAFS spectra and XRD patterns]. See DOI: 10.1039/x0xx00000x

transmission electron microscopy (HAADF-STEM), energy dispersive X-ray spectroscopy (EDS) and *in situ* synchrotron X-ray diffraction (XRD) were used to determine the structure of the bimetallic nanoparticles.

Materials and methods

Materials

Davisil 636 silica gel (99%), $H_2PtCl_6 \cdot 6H_2O$ (99.9%), $BiCl_3$ (99.999%), $Pt(NH_3)_4(NO_3)_2$ (99.995%), $Bi(NO_3)_3 \cdot 5H_2O$ (99.999%) were purchased from Sigma-Aldrich and used without further purification. ZSM-5 (Si/Al=40) of ammonium form was from Zeolyst International. The gases used for the catalytic testing were purchased from Indiana Oxygen Company, and the C_3H_8 is 5% balanced with N_2. The H_2 was also 5% balanced with N_2. Ultra-high purity gases were N_2 (99.999%) and He (99.98%). The gases used for XAS and XRD experiments were purchased from AirGas, Illinois, and all the gases were balanced with He.

Catalyst preparation

Pt-Bi bimetallic catalysts on silica with target Pt loading of 2 wt% were synthesized by a sequential incipient wetness impregnation (IWI). 0.2 g $Pt(NH_3)_4(NO_3)_2$ was dissolved in 3.5 mL DI water. The obtained solution was added dropwise to 5.0 g Silica (Davisil 636 silica gel, 480 m^2/g, 0.75 mL/g pore volume) with continuous stirring. Pt/SiO_2 was dried at 100 °C overnight followed by calcination at 400 °C for 4 hours. Different amounts of $Bi(NO_3)_3 \cdot 5H_2O$ was dissolved in 3.5 mL 2 mol/L nitric acid. The solution was added dropwise to the Pt/SiO_2 catalyst. The obtained catalysts were dried overnight at 100 °C and calcined at 400 °C for 4 h. These samples are referenced as xBi-2Pt/SiO_2, where x denotes as x wt% of Bi loading. For comparison, the monometallic 2Pt/SiO_2 catalyst with 2 wt% Pt loading was also prepared using the same method.

ZSM-5 (Si/Al=40) of ammonium form (CBV 8014, 425 m^2/g) was calcined at 550 ℃ for 4 hours to transform into H-form. Pt-Bi bimetallic catalysts on ZSM-5 with target Pt loading of 1 wt% were synthesized by a sequential wet impregnation. $H_2PtCl_6 \cdot 6H_2O$ was dissolved in HCl (pH=5-6) solution and added dropwise to HZSM-5 slurry, with stirring at room temperature for 8 hours. Pt/HZSM-5 was dried at 100 °C overnight followed by calcination 400 °C for 4 hours. Various amounts of $BiCl_3$ were dissolved in HCl solution (pH=5-6) and added dropwise to Pt/HZSM-5. The obtained catalysts were dried overnight at 100 °C and calcined at 400 °C for 4 h. These samples are named as xBi-1Pt/ZSM-5, where x denotes as x wt% of Bi loading. For comparison, the monometallic 1Pt/ZSM-5 catalyst with 1 wt% Pt loading was also prepared using the same method. These catalysts were shown to have similar activity, C_2^+ selectivity and stability for NOCM as previously reported. [18]

In situ X-ray diffraction (XRD)

The XRD measurements were performed at 11-ID-C beamline at the Advanced Photon Source (APS) in Argonne National Lab. X-rays at 105.715 keV (λ=0.11730Å) were used to acquire the XRD patterns. Catalyst samples were pressed into small pellets and placed into a Linkam Thermal Stage to perform the XRD measurements. The stage was purged with He at room temperature. 5% H_2/He at 50 cc/min was introduced to the stage and the temperature was ramped to 550 °C. After reduction for 30 min, the diffraction pattern was collected at 550 °C. After cooling the sample to room temperature, the diffraction pattern was collected. The diffraction data for the empty stage and silica support was also collected with the same procedure for background subtraction. The obtained 2-D diffraction patterns were converted to 1-D patterns of intensity versus 2θ by the Fit2D software. The diffraction patterns of Pt (ICSD:9012957)[19], Pt_1Bi_1 (ICSD:9008911)[20], Pt_1Bi_2 (ICSD:9012345)[21], Bi (ICSD:2310889)[22] were simulated by using standard patterns with Materials Analysis Using Diffraction (MAUD) v. 2.5.5 software. The XRD simulation of Pt_1Bi_1 and Pt_3Bi intermetallic alloy was based on the proposed crystal structure.

In situ X-ray absorption spectroscopy

The XAS measurements were performed at 10-BM beamline at the APS. Measurements were carried out in step-scan transmission mode in about 10 min. Samples were pressed in a cylindrical sample holder containing six wells to form self-supported catalyst wafers. The sample holder was placed in a quartz tube with ports containing Kapton windows so samples could be treated prior to measurements. The catalysts were pre-reduced in 100 cc/min of 3% H_2/He at 550 °C before taking the spectra at room temperature.

XAS data was fitted by using Demeter 0.9.25 software package. The edge energy was determined using the maximum of the first peak in the first derivative of the XANES spectra. Least-squares fit in R-space of the k^2-weighted Fourier transform data from 3.0 to 12.0 $Å^{-1}$ was used to obtain the EXAFS coordination parameters. The first shell was used to fit the EXAFS spectra. The amplitude reduction factor (S_0^2) was determined as 0.80 by fitting a reference spectrum of the Pt foil, and then it was used for fitting of all the other EXAFS spectra. One Pt and Bi path were included, and eight free parameters were used for the initial fitting. With the information of the Pt_3Bi_1 structure, three-path fitting was carried out by fixing one Pt-Pt path as an equal distance as one Pt-Bi path, and the ratio of the coordination numbers of the two paths was set as 2:1 consistent with the Pt_3Bi crystal structure.

STEM

STEM experiments were conducted using the FEI Talos F200X scanning transmission electron microscope with a high angle annular dark field (HAADF) detector at 200 kV. The atomic resolution microscopy analysis and elemental mapping was performed on the JEM ARM200F microscope with a probe Cs-corrector working at 200 kV. The samples were reduced in H_2 at 550 °C for 30 min and exposed to air at the room temperature before the STEM measurement. The samples were grounded and dispersed in isopropanol. Then the suspension was dropped on copper TEM ready grids (TedPella) and dried on a hot plate. The particle size distribution was determined by counting 200 particles per sample using Nano Measurer 1.2.

CO FTIR

2 | *Catal. Sci. Technol.*, 2018, **00**, 1-3

This journal is © The Royal Society of Chemistry 20xx

In situ Fourier Transform Infrared spectra were acquired with a Bruker TENSOR27 spectrometer equipped with a mercury cadmium telluride detector in transmission mode between 1000 cm^{-1} and 4000 cm^{-1} with 32 scans and a resolution of 4 cm^{-1}. About 30 mg of the sample was pressed to a disk with a diameter of 13 mm. The samples were pretreated in 50 mL/min of N_2 at 120 °C for 10 min and then cooled down to room temperature to collect the background spectrum. 5% CO/He was then flowed in the sample disk for 5~10 min until the intensity of gaseous peaks didn't change. Subsequently, the gas was switched to N_2 (50 mL/min) to collect the spectra until the CO gaseous peaks disappeared. Then the samples were reduced in 50 mL/min H_2 at 500 °C for 20 min. Finally, the samples were cooled down to room temperature and the CO adsorption and N_2 blowing processes were repeated.

CO chemisorption

CO chemisorption was performed on a Micromeritics ASAP 2020 chemisorption instrument. Around 0.1 g catalysts were weighted and loaded into a U-shaped quartz reactor. 50 cc/min of 5% H_2/He was introduced into the reactor to reduce the catalysts at 550 °C and cooled to RT. He was flushed for 30 min before evacuation and measurements. The catalyst dispersion was obtained by difference analysis in the chemisorption curve. A stoichiometry of CO: Pt = 1:1 was assumed to calculate the dispersion for the catalysts.

Propane dehydrogenation catalytic performance tests

Propane dehydrogenation catalytic performance was tested in a quartz tube reactor (I.D. = 9.5 mm) connected to Agilent 6890 gas chromatograph. A K-type thermocouple (O.D. = 3.2 mm) was placed in the center of the catalyst bed to measure the temperature of the catalyst. A furnace connected to a controller was used to maintain the desired temperature. The catalyst was diluted with Davisil 636 silica gel to maintain the catalyst bed height at ~12.7 mm. The criteria by Weisz and Prater [23] and Mears [24] were both satisfied (details are shown in SI), confirming the absence of heat-transfer and mass-transfer effects in all measurements.

Prior to the reaction, the catalysts were reduced at 550 °C at 50 mL/min 5% H_2 and balance N_2 while temperature was ramped from room temperature to 550 °C at 10 °C/ min and held at 550 °C for 30 min. The reaction temperature was 550 °C and the reactants were 2.5% C_3H_8, 2.5% H_2 and balance N_2. The gas hourly space velocity (GHSV) was adjusted to determine the selectivity at certain conversions. A Carboxen-1010 PLOT capillary GC Column was used to separate the components in the reactor effluent gas mixture. Selectivity was calculated by C_3H_6/(total carbon - C_3H_8) × 100%.

Results and discussion

The Pt L_3 edge X-ray Absorption near edge structure (XANES) spectra of Pt-Bi on ZSM-5 with different Bi loadings are shown in Figure 1 (A). These catalysts had similar catalytic performance for NOCM as previously reported. [18] The white line intensity is typical of fully reduced metallic Pt in all catalysts. The edge energies determined by the inflection point of the leading edge are given in Table S1. The edge energy of
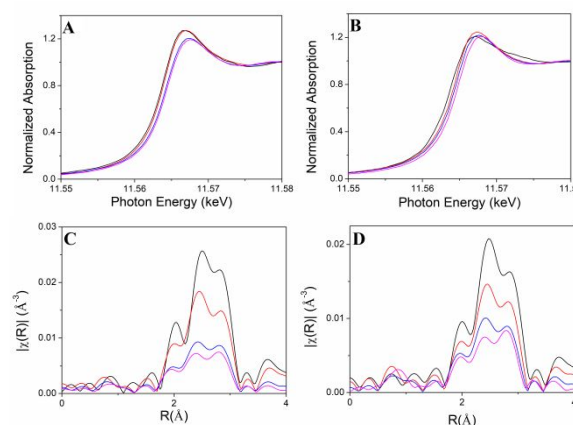

Figure 1. (A) Pt L$_{III}$ edge XANES spectra of Pt-Bi/ZSM-5. (B) Pt L$_{III}$ edge XANES spectra of Pt-Bi/SiO$_2$ (C) k^2-weighted Fourier transformation magnitude of the EXAFS spectra of Pt-Bi/ZSM-5. k^2-weighted FT k-range of 3.0 – 12.5 Å^{-1}. (D) k^2-weighted Fourier transformation magnitude of the EXAFS spectra of Pt-Bi/SiO$_2$. k^2-weighted FT k-range of 3.0 – 12.5 Å^{-1}. For (A) and (C): 1Pt/ZSM-5 (black), 0.1Bi-1Pt/ZSM-5 (red), 0.8Bi-1Pt/ ZSM-5 (blue) and 1Bi-1Pt/ZSM-5 (magenta). For (B) and (D): 2Pt/SiO$_2$ (black), 1Bi-2Pt/SiO$_2$ (red), 2Bi-2Pt/SiO$_2$ (blue) and 4Bi-2Pt/SiO$_2$ (magenta).

0.1Bi-1Pt/ZSM-5 was 0.1 eV higher than monometallic Pt; while those of 0.8Bi-1Pt/ZSM-5 and 1Bi-1Pt/ZSM-5 were 0.6 eV higher. The shift in XANES energy and change in the shape of the white line suggest that Pt and Bi form bimetallic nanoparticles.

The atomic numbers of Pt and Bi differ only by 5; therefore, scattering from Pt-Pt and Pt-Bi at the same bond distance shows only slight differences in the k space extended X-ray absorption fine structure (EXAFS) spectra as shown in Figure S1 (B). Although there are minor differences, these are not generally large enough to resolve the contributions in the EXAFS. If however, the Pt-Pt and Pt-Bi bond distances are different, the differences in EXAFS are larger (Figure S1) and can be resolved in the fits.

Three main peaks in k^2-weighted magnitude of the Fourier transform of Pt/ZSM-5 shown in Figure 1 (C) are typical Pt-Pt scattering of metallic Pt nanoparticles. The peak positions and relative intensities, however, change with increasing Bi loading suggesting the presence of Bi scattering

Table 1. EXAFS fitting parameters for Pt-Bi/ZSM-5

Sample Name	Scattering Pair[a]	CN	Bond distance (Å)	σ² (Å²)
1Pt/ZSM-5	Pt-Pt	10.2	2.74±0.02	0.004
0.1Bi-1Pt/ZSM-5	Pt-Pt	9.4	2.75±0.01	0.005
	Pt-M	1.1	2.81±0.05	0.009
0.8Bi-1Pt/ZSM-5	Pt-Pt	6.1	2.75±0.01	0.006
	Pt-M	2.7	2.81±0.03	0.005
1Bi-1Pt/ZSM-5	Pt-Pt	4.8	2.75±0.01	0.005
	Pt-M	3.4	2.80±0.04	0.009

[a] M = Pt or Bi (Bi was used for FEFF calculations.)

neighbors within the bonding distance. Despite the similar particle sizes[18], the magnitude of the Fourier transform decreases with increasing the Bi loading likely indicating the presence of destructive interference of the EXAFS.

The fit of the EXAFS at Pt edge of the Pt-Bi/ZSM-5 catalysts are given in Table 1. The 2Pt/ZSM-5 has a Pt-Pt coordination number of 10.2. The Pt-Pt bond distance is 2.74 Å, in agreement with the Pt nanoparticles. For Pt-Bi catalysts, fits of the EXAFS with a single scattering distance were poor. Using two scattering paths, a Pt-Pt bond distance at 2.75 Å, and a second scattering path of Pt-M, where M could be Pt or Bi, at a bond distance of 2.81 Å gave good fits. The Pt-M coordination number increased with increasing Bi loading suggesting M is likely Bi. The Pt-Pt coordination number is larger than Pt-M, which suggests Pt-rich bimetallic Pt-Bi nanoparticles.

To study the crystal phase of the bimetallic nanoparticles, diffraction is needed. The XRD spectra of Pt-Bi/ZSM-5 shown in the previous study, however, have large ZSM-5 peaks, which obscure the weak Pt-Bi metallic nanoparticle peaks. [18] Therefore, Pt and Pt-Bi catalysts of similar composition were synthesized on amorphous SiO_2 support to allow nanoparticle diffraction to be resolved. The STEM images of the Pt-Bi/SiO_2 catalysts are shown in Figure S2. The average particle size is 2-3 nm, Table 2 and Figure S3, which are similar to those in Pt-Bi/ZSM-5.[18] The infrared spectra also show linear bonded CO at similar frequencies, Figure S4.

The bimetallic nanoparticles on Pt-Bi/SiO_2 catalysts are very similar to the ones on Pt-Bi/ZSM-5 according to XAS. The Pt L_3 XANES spectra and edge energies of the Pt-Bi/SiO_2 are shown in Figure 1 (B) and Table S1, respectively. Compared with Pt/SiO_2, the edge energies of 2Pt-1Bi/SiO_2, 2Pt-2Bi/SiO_2 and 2Pt-4Bi/SiO_2 were shifted to higher energy, 0.6 eV, 0.7 eV and 0.8 eV, respectively. The increase in the XANES energy with increasing Bi loading is similar to that in Pt-Bi/ZSM-5. The k^2-weighted magnitude of the Fourier transform of the Pt-Bi/SiO_2 catalysts are shown in Figure 1 (D) and decrease with increasing Bi loading very similar to that on ZSM-5 (Figure 1 (C)). The Pt-Pt coordination number was 8.7 and the bond distance was 2.73 Å, similar to 1Pt/ZSM-5. For Pt-Bi/SiO_2 catalysts (Table 3), the catalysts were fit using two scattering paths. The Pt-Pt bond distance is 2.74-2.76 Å, which is similar to Pt-Bi/ZSM-5. A

Table 3. EXAFS fitting parameters for Pt-Bi/SiO_2

Sample Name	Scattering Pair[a]	Coordination Number	Bond distance (Å)	σ^2 (Å^2)
2Pt/SiO_2	Pt-Pt	8.7 ± 0.1	2.73 ± 0.01	0.007
1Bi-2Pt/SiO_2	Pt-Pt	8.5 ± 1.7	2.74 ± 0.01	0.006
	Pt-M	1.1 ± 6.4	2.79 ± 0.15	0.012
2Bi-2Pt/SiO_2	Pt-Pt	5.6 ± 0.9	2.74 ± 0.03	0.006
	Pt-M	1.6 ± 3.5	2.79 ± 0.10	0.008
4Bi-2Pt/SiO_2	Pt-Pt	1.8 ± 0.9	2.76 ± 0.04	0.005
	Pt-M	4.2 ± 1.0	2.78 ± 0.03	0.009

[a] M = Pt or Bi (Bi was used for FEFF calculations.)

second scattering path of Pt-M (M is Pt or Bi) at a bond distance of 2.79 Å gave good fits. The Pt-M coordination number increases as the Bi loading increases consistent with M being Bi. The k space and R space EXAFS spectra of 2Bi-2Pt/SiO_2 and 0.8Bi-1Pt/ZSM-5 have nearly identical spectra (Figure S5), and suggest that the Pt-Bi nanoparticle structures on silica and ZSM-5 are similar.

To further investigate the phase assemblage of the Pt-Bi bimetallic nanoparticles, *in situ* synchrotron XRD patterns were obtained on Pt-Bi/SiO_2 at 550 °C (Figure 2 (A)). The energy of the X-ray beam is 105.715 keV, resulting in diffraction peaks at low two Theta angle. 2Pt/SiO_2 showed peaks at 2.980°, 3.430°, 4.881°, and 5.712° corresponding to the (111), (200), (220) and (311) planes of the Pt face-centered cubic (FCC) structure. For the Pt-Bi catalysts, the peaks shift slightly to lower two Theta angles with increasing Bi loadings (Table S2), indicating lattice expansion caused by Bi incorporation due to the larger size of Bi than Pt, with atomic radii 1.56 and 1.39 Å, respectively.[25] In addition, the diffraction patterns of the Pt-Bi catalysts remain similar to the Pt catalyst. The relative peak positions and intensity are characteristic of FCC lattice. This suggests either formation of FCC Pt-Bi solid solution, or an intermetallic alloy with superlattice based on the FCC lattice. The former is not likely since the solubility of Bi in Pt is less than 1%,[26] which is inconsistent with the EXAFS fits in Tables 1 and 3 suggesting much higher Bi content. Solid solutions with high solubility generally form between two metals having the same

Table 2. Propane dehydrogenation, CO chemisorption and STEM Particle Size[a]

Sample Name	C_3H_6 Selectivity (%)	Particle size (nm)[b]	Pt Dispersion (%)[c]	Initial Turnover Rate (s^{-1})[d]
2Pt/SiO_2	60	2.7 ± 0.5	30.2	0.22
1Bi-2Pt/SiO_2	90	2.3 ± 0.5	8.2	0.43
2Bi-2Pt/SiO_2	87	2.2 ± 0.4	6.5	0.58
4Bi-2Pt/SiO_2	87	2.7 ± 0.4	4.4	0.31

[a] Reaction conditions: 550 °C, 2.5 % C_3H_8 + 2.5 % H_2 balanced with N_2; selectivity and TOR calculated at 10% C_3H_8 conversion. [b] Particle size calculated from STEM. [c] Pt dispersion calculated by CO chemisorption. [d] TOR calculated based on C_3H_8 conversion rate.
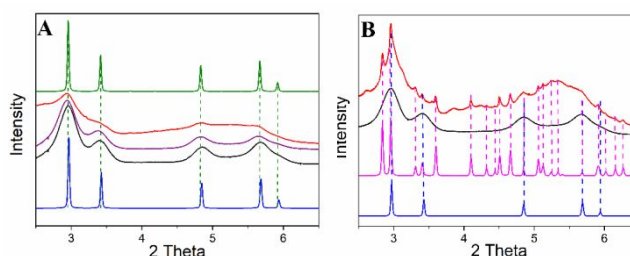

Figure 2. (A) *In Situ* XRD patterns taken at 550 °C (X-ray energy=105.715 keV). (B) *In Situ* XRD patterns taken at room temperature (X-ray energy=105.715 keV). Pt simulation (blue, ICSD 9012957), Bi simulation (magenta, ICSD 2310889), Pt_3Bi simulation (olive),1Bi-2Pt/SiO_2 (black), 2Bi-2Pt/SiO_2 (purple), 4Bi-2Pt/SiO_2 (red).
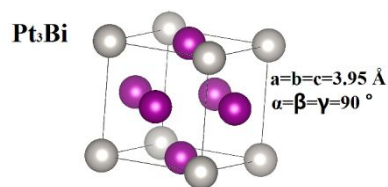
4 | *Catal. Sci. Technol.*, 2018, **00**, 1-3

This journal is © The Royal Society of Chemistry 20xx

Figure 3. Structure of the simulated Pt_3Bi structure

Figure 5. (A) The high resolution HAADF image and elemental distribution of (B) Bi, (C) Si , (E) Pt , and (F) O as revealed by EDS analysis. The core-shell configuration has been clearly demonstrated by (D) the mix-over image of Pt M and Bi M signals.

lattice type (for example, FCC).[27] Though Pt is FCC, Bi is rhombohedral. In addition, the average Pt-Bi bond distance would be the sum of the radii of Pt and Bi or 2.95Å for a solid solution with 50% Bi. The experimental bond distance is much shorter at 2.80 Å, suggesting the presence of strong Pt-Bi bonds consistent with the formation of an intermetallic alloy. Finally, previous studies on similar nanoparticles between Pt and a second metal, including In[28], Mn[29] and Sb[30] shows that incorporation of the second metal into the Pt nanoparticles are diffusion limited due to the strong Pt-M bonds, leading to intermetallic transformation starting from the surface layers, which is consistent with our interpretation of the characterization data on Pt-Bi catalysts. Thus, the bimetallic Pt-Bi is not a solid solution.

For possible intermetallic phases, the two thermodynamically stable bulk phases, Pt_1Bi_1,[20] Pt_1Bi_2[21] (Figure S6 (A)) do not have FCC type lattice, and their XRD peak positions do not match those of the Pt-Bi bimetallic nanoparticles. Thus, neither is the structure of these nanoparticles. *Since the bimetallic Pt-Bi nanoparticles are not solid solutions, nor known bulk alloy structures, it is possible that there is a new nano-phase intermetallic alloy structure.* Recently, several intermetallic nanoparticle alloy catalysts with AuCu structure, or closely related cubic structure, have been determined for Pt_1Zn_1,[31] β_1-PdZn[32] and Pd_1In_1.[28] For each of these, the nano-alloy phase is known in the bulk phase diagram. However, recently, Ye et al. identified a surface tetragonal Pt_1Sb_1 intermetallic nanoparticle phase with AuCu structure type, which does not exist in the bulk.[30] A simulated Pt_1Bi_1 XRD pattern based on the same type of AuCu tetragonal structure (Pt-M at 2.81 Å and Pt-Pt at 2.74 Å) is shown in figure S6 (B). This structure also does not match the diffraction peaks of the Pt-Bi catalysts.

In the previous study by Gercecker et al.[17] Pt-Sn supported on SiO_2 and ZSM-5 was catalytic for NOCM, and Pt-Sn is known to have an Cu_3Au type intermetallic Pt_3Sn[33-35] structure. In this Pt_3M
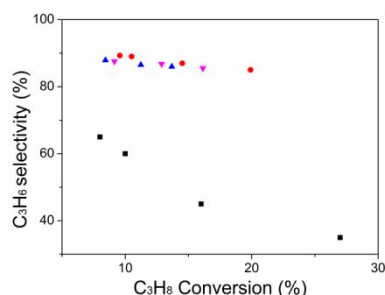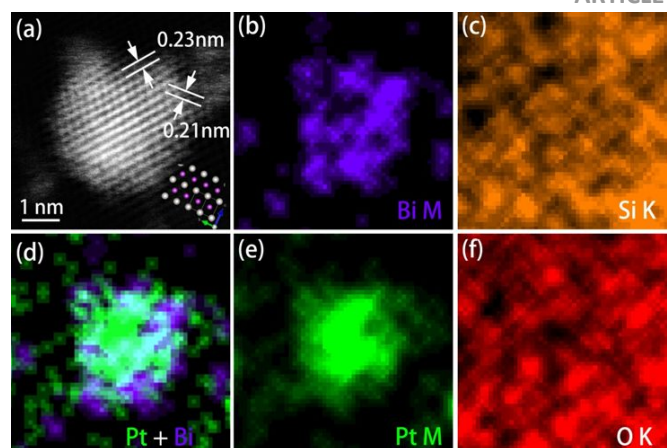

Figure 4. Propylene selectivity at different conversions of $2Pt/SiO_2$ (black), $1Bi-2Pt/SiO_2$ (red), $2Bi-4Pt/SiO_2$ (blue) and $4Bi-2Pt/SiO_2$ (magenta). Reaction conditions: 550 °C, 2.5 % C_3H_8 + 2.5 % H_2 balanced with N_2.

structure, Pt-Pt and Pt-M bond distances and the XRD patterns are very similar. A simulation of Cu_3Au type Pt_3Bi phase with Pt-M with bond distances at 2.81 Å and second monometallic Pt phase with bonds at 2.74 Å, which are consistent with the EXAFS fits, gave an XRD pattern that matches the experimental peak positions in Figure 2 (A). Because the atomic number of Pt and Bi are similar, the superlattice peaks are too weak to be seen even in the simulation. Nevertheless, based on the EXAFS and XRD results, the bimetallic Pt-Bi nanoparticle is proposed to consist of two phases: Pt_3Bi (Figure 3) and unalloyed Pt, i.e., a Pt-rich Pt-Bi bimetallic nanoparticle.

Several possibilities exist for the two metallic phases in the Pt-Bi catalysts. These could be two separate phases, e.g., Pt and Pt_3Bi, a core-shell morphology, for example, Pt_3Bi on a Pt core, or the inverse. In order to determine the location of the alloy phase, the catalytic performance for propane dehydrogenation was determined for the Pt-Bi/SiO_2 catalysts. Hydrogen was co-fed with propane to increase the hydrogenolysis selectivity to light alkanes, e.g., methane, ethane and ethylene, and provides a more severe test of the catalysts' olefin selectivity. The propylene selectivity are shown in Figure 4 and Table 2 (at 10% conversion).

The propylene selectivity at 10% conversion for $2Pt/SiO_2$ was 60%; while for Pt-Bi bimetallic catalysts the selectivity was ca. 90%. The propylene selectivity for monometallic Pt decreased rapidly with increasing conversion; while the propylene selectivity for Pt-Bi bimetallic catalysts remained nearly constant at about 90% as the conversion increased. As the Bi loading increases from 1-4%, there is little change in the propylene selectivity. The high olefin selectivity at low promoter loading suggests a Pt_3Bi intermetallic surface alloy on a Pt core,[36] similar to other intermetallic alloys.[28, 31, 33, 37]

HAADF image (Figure 5(A)) reveals the atomic structure of an individual Pt-Bi particle in 0.8Bi-1Pt/ZSM-5. The EDS provides intuitive elemental distribution of Pt and Bi, where a Pt-Bi alloy shell in thickness of ~1 nm could be confirmed outside a 1 nm Pt-rich core. The lattice spacing of 0.23 nm and 0.21 nm at the shell can be indexed to be (111) and (200) planes of a typical FCC phase. In addition, the line-distribution of Pt and Bi (Figure S7) shows the fact of a Pt-Bi alloy shell encapsulating outside a Pt-rich core. High-

resolution HAADF image (Figure 5(A)) shows FCC atomic arrangement symmetry suggesting the Pt₃Bi structure for the shell and the metallic Pt core. The above structural evidences coincide with the propane dehydrogenation analysis serving as additional real-space microscopic evidence for the unique core-shell configuration of the Pt-Bi particle.

The turnover rates (TORs), i.e., rate per surface Pt, under differential conditions are also given in Table 2. The initial TORs of Pt-Bi/SiO$_2$ are very similar to that of 2Pt/SiO$_2$ at 550°C. However, at higher reaction temperature, or reduction at higher temperatures and reaction at 550°C, the rates per gram of catalyst were much lower. The XRD pattern of 4Bi-2Pt/SiO$_2$ taken at 550 °C, Figure 2 (A) (red), showed broad peaks typical of the surface Pt$_3$Bi on Pt core structure of the Pt-Bi catalysts. However, upon cooling the pattern collected at room temperature showed many additional sharp features, Figure 2 (B) (red). These new peaks match those of metallic Bi. Thus, at high Bi loading and high reduction temperatures, excess Bi$_2$O$_3$ reduces to metallic Bi as liquid form (melting point of Bi is 271.5°C[38]). The loss of catalytic activity is likely due to covering of the catalytic Pt$_3$Bi with non-catalytic, metallic Bi.

At lower Bi loading, for example, 1% Bi, Figure 2 (B) (black), there are no metallic Bi peaks in the XRD at room temperature. These results suggest that for Pt-Bi, low Bi loadings and low reduction temperatures are required to maintain catalytic activity. At high Bi loading, or reduction temperatures, excess Bi is reduced, mobile and covers active sites. These results for Pt-Bi/SiO$_2$ are consistent with the Pt-Bi/ZSM-5 NOCM catalysts, where high Bi loading, or high reaction temperature leads to poor activity.[18]

The structures of the Pt-Bi bimetallic catalysts with different Bi loadings are schematically shown in Figure 6, where at very low loading, e.g. about 0.1%, there is little surface Pt$_3$Bi and most of the surface is monometallic Pt. This catalyst has catalytic properties similar to Pt, i.e. poor selectivity and stability. At loadings sufficient to produce a Pt$_3$Bi monolayer, the alkane dehydrogenation (on SiO$_2$) and NOCM (on ZSM-5) selectivity and stability are higher. With high Bi loading, metallic Bi is more easily reduced and covers the catalytic surface. For all catalysts, the non-reduced Bi$_2$O$_3$ present in all catalysts is reduced to metallic Bi at high temperature leading to inactive catalysts. Similar bimetallic structure evolution has been reported for Pd-In[28] and Pd-Zn[32] catalysts.

Conclusions

In summary, the structure of Pt-Bi/ZSM-5 NOCM catalyst is similar to Pt-Bi/SiO$_2$. EXAFS indicates the formation of Pt-rich bimetallic Pt-Bi nanoparticles with Pt-Bi bond distance of 2.80 Å. The XRD spectra (on SiO$_2$) are consistent with cubic, intermetallic surface Pt$_3$Bi phase on a Pt core. The Pt$_3$Bi structure is not known in
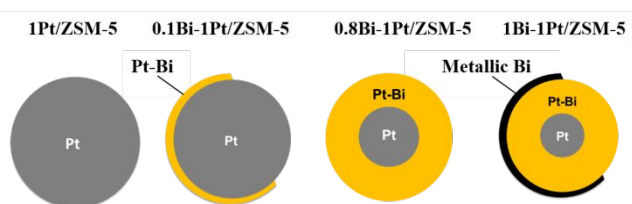

Figure 6. Schematic model of geometric structure of the Pt and Pt–Bi catalysts.

the thermodynamic phase diagram. In all catalysts, only a small fraction of Bi alloys with Pt. At high Bi loadings, excess Bi reduces at high temperature, covering the catalytic surface leading to a loss in activity. At lower Bi loadings with little excess Bi, the Pt$_3$Bi surface is effective for NOCM (on ZSM-5) and propane dehydrogenation (on SiO$_2$).

The current study along with the previous report for NOCM by Pt-Sn catalysts[17] suggests that Pt intermetallic alloys are significantly more selective than monometallic Pt.[16] Both Pt-Sn[33, 34] and Pt-Bi bimetallic compositions have Pt$_3$M surface structures, suggesting that other Pt$_3$M alloys, and perhaps other noble metal intermetallic structures, may also be selective for NOCM. In addition, both bimetallic compositions are selective for alkane dehydrogenation. Although NOCM requires the catalyst to form a C-C bond while alkane dehydrogenation does not, these results suggest noble metal intermetallic alloys have high selectivity for both reactions. Finally, high equilibrium conversions of NOCM require very high reaction temperature, typically, up to about 900-1000°C. For Bi, at these temperatures, excess Bi$_2$O$_3$ is reduced and covers the active Pt site leading to loss of activity. For high selectivity and conversion, alloys with promoter metals, that form Pt$_3$M and are not reduced under these extreme conditions may lead to better performance.

Acknowledgement

Conflicts of interest

The authors declare no conflict of interest.

Notes and references

1   B. Hu, N. M. Schweitzer, G. Zhang, S. J. Kraft, D. J. Childers, M. P. Lanci, J. T. Miller and A. S. Hock, *ACS Catal.*, 2015, **5**, 3494-3503.
2   V. J. Cybulskis, S. U. Pradhan, J. J. Lovón-Quintana, A. S. Hock, B. Hu, G. Zhang, W. N. Delgass, F. H. Ribeiro and J. T. Miller, *Catal. Lett.*, 2017, **147**, 1252-1262.
3   J. J. Siirola, *AIChE J.*, 2014, **60**, 810-819.
4   P. Schwach, X. Pan and X. Bao, *Chem. Rev.*, 2017, **117**, 8497-8520.
5   T. Ito and J. H. Lunsford, *Chem. Rev.*, 1985, **314**, 721-722.

6 | *Catal. Sci. Technol.*, 2018, **00**, 1-3

This journal is © The Royal Society of Chemistry 20xx

ARTICLE

6   B. Yingli, Z. Kaiji, J. Yutao, T. Chiwen and Y. Xiangguong, *Appl. Cat.*, 1988, **39**, 185-190.

7   R. Ghose, H. T. Hwang and A. Varma, *Appl. Cat. A*, 2014, **472**, 39-46.

8   S. Arndt, G. Laugel, S. Levchenko, R. Horn, M. Baerns, M. Scheffler, R. Schlögl and R. Schomäcker, *Cat. Rev.*, 2011, **53**, 424-514.

9   L. Wang, L. Tao, M. Xie, G. Xu, J. Huang and Y. Xu, *Cat. Lett.*, 1993, **21**, 35-41.

10   N. Kosinov, F. J. Coumans, E. A. Uslamin, A. S. Wijpkema, B. Mezari and E. J. Hensen, *ACS Catal.*, 2016, **7**, 520-529.

11   Y. Xu, Y. Song, Y. Suzuki and Z.-G. Zhang, *Catal. Sci. & Technol.*, 2014, **4**, 3644-3656.

12   S. Majhi and K. Pant, *J. Ind. Eng. Chem.*, 2014, **20**, 2364-2369.

13   S.-T. Wong, Y. Xu, L. Wang, S. Liu, G. Li, M. Xie and X. Guo, *Catal. Lett.*, 1996, **38**, 39-43.

14   L. Nykänen and K. Honkala, *ACS Catal.*, 2013, **3**, 3026-3030.

15   X. Guo, G. Fang, G. Li, H. Ma, H. Fan, L. Yu, C. Ma, X. Wu, D. Deng and M. Wei, *Science*, 2014, **344**, 616-619.

16   M. Belgued, P. Pareja, A. Amariglio and H. Amariglio, *Nature*, 1991, **352**, 789-790.

17   D. Gerceker, A. H. Motagamwala, K. R. Rivera-Dones, J. B. Miller, G. W. Huber, M. Mavrikakis and J. A. Dumesic, *ACS Catal.*, 2017, **7**, 2088-2100.

18   Y. Xiao and A. Varma, *ACS Catal.*, 2018, **8**, 2735-2740.

19   E. Owen and E. Yates, *Philos. Mag.*, 1933, **15**, 472-488.

20   R. Wyckoff, *Cryst. Struct.*, 1963, **1**, 85-237.

21   N. E. Brese and H. G. von Schnering, *Z. Anorg. Allg. Chem.*, 1994, **620**, 393-404.

22   P. Cucka and C. Barrett, *Acta Crystallogr.*, 1962, **15**, 865-872.

23   P. B. Weisz and C. Prater, *Adv. Catal.*, 1954, **6**, 143-196.

24   D. E. Mears, *J. Cat.*, 1971, **20**, 127-131.

25   J. C. Slater, *J. Chem. Phys.*, 1964, **41**, 3199-3204.

26   H. Okamoto, *J. Phase Equilib.*, 1991, **12**, 207-210.

27   W. Hume-Rothery and H. M. Powell, Z. Kristallogr. Cryst. Mater., 1935, **91**, 23-47.

28   Z. Wu, E. C. Wegener, H.-T. Tseng, J. R. Gallagher, J. W. Harris, R. E. Diaz, Y. Ren, F. H. Ribeiro and J. T. Miller, *Catal. Sci. Technol.*, 2016, **6**, 6965-6976.

29   Z. Wu, B. C. Bukowski, Z. Li, C. Milligan, L. Zhou, T. Ma, Y. Wu, Y. Ren, F. H. Ribeiro and W. N. Delgass, J. Am. Chem. Soc., 2018, **140**, 14870–14877.

30   C. Ye, Z. Wu, W. Liu, Y. Ren, G. Zhang and J. T. Miller, *Chem. Mater.*, 2018, **30**, 4503-4507.

31   V. J. Cybulskis, B. C. Bukowski, H.-T. Tseng, J. R. Gallagher, Z. Wu, E. Wegener, A. J. Kropf, B. Ravel, F. H. Ribeiro, J. T. Miller and J. Greeley, *ACS Catal.*, 2017, **7**, 4173-4181.

32   J. R. Gallagher, D. J. Childers, H. Zhao, R. E. Winans, R. J. Meyer and J. T. Miller, *Phys. Chem. Chem. Phys.*, 2015, **17**, 28144-28153.

33   L. Deng, H. Miura, T. Shishido, S. Hosokawa, K. Teramura and T. Tanaka, *ChemCatChem*, 2014, **6**, 2680-2691.

34   J. Llorca, N. Homs, J.-L. G. Fierro, J. Sales and P. R. de la Piscina, *J. Catal.*, 1997, **166**, 44-52.

35   B. K. Vu, M. B. Song, I. Y. Ahn, Y.-W. Suh, D. J. Suh, W.-I. Kim, H.-L. Koh, Y. G. Choi and E. W. Shin, *Catal. Today*, 2011, **164**, 214-220.

36   Z. Ma, Z. Wu and J. T. Miller, *Catal., Struct. React.*, 2017, **3**, 43-53.

37   E. C. Wegener, Z. Wu, H.-T. Tseng, J. R. Gallagher, Y. Ren, R. E. Diaz, F. H. Ribeiro and J. T. Miller, *Catal. Today*, 2018, **299**, 146-153.

38   W. Klement Jr, A. Jayaraman and G. Kennedy, *Phys. Rev.*, 1963, **131**, 632.

This journal is © The Royal Society of Chemistry 20xx

Catal. Sci. Technol., 2018, **00**, 1-3 | **7**

Cubic Pt$_3$Bi Shell

FCC Pt Core

Pt@Pt$_3$Bi